2016 Conductivity Anomaly , 28-34

Understanding Negative Apparent Conductivity Response In Low Induction Number Electromagnetic Instruments

（ローインダクションナンバー電磁探査器による負の電気伝導度読み値に対する解釈）

Ame Thato Selepeng*, Shin'ya Sakanaka, Tadashi Nishitani
Faculty of International Resource Sciences, Akita University
*E-mail: d9512001@wm.akita-u.ac.jp

ABSTRACT

Under certain geological conditions, low induction number electromagnetic (LIN-EM) instruments are known to produce negative apparent conductivity (σ_a) responses. This is particularly the case when the shallow subsurface is characterized by highly conductive bodies, however little attention has been given to this issue in the research literature. To analyse negative σ_a anomalies and their causative structures, we make use of a 3-D integral equation forward modeling technique based on a 3-D weighting function. We present 3-D numerical modeling results over a volcanic tuff body intruded by several dacite dikes, in Daisen City, Japan. Our 3-D model resolved the horizontal and vertical extent of the dacite dikes and also delineated a high conductive zone between the volcanic tuff and the intrusive dacite dikes. This zone is the causative structure for negative σ_a responses in the VMD data, and is interpreted to be an alteration zone. The true conductivity model achieved by 3-D forward modeling is shown to compare favourably with the DC resistivity data acquired in the same area.

INTRODUCTION

The occurrence of negative σ_a anomalies in LIN-EM instruments was first reported by McNeill (1983) for his studies on the EM response of a conductive vertical dike. He observed that for high true ground conductivity (σ), the indicated σ_a on the meter exhibited negative response in the VMD mode but was unresponsive in the HMD mode in the vicinity of the conductive dike. Until recently, quantitative analysis of loop-loop EM data has mostly been limited to 1-D forward modeling and inversion. However in order to handle negative σ_a data, 1-D equations are not applicable because such anomalies are caused by 2-D or 3-D effects of the subsurface structure. Pérez-Flores et al. (2012) published a 3-D imaging technique for EM measurements based on a 3-D weighting function assuming LIN conditions. We extend the findings by Pérez-Flores et al. (2012) by modeling real field data exhibiting negative σ_a anomalies from a dacite dike intrusion in Sugisawa, Daisen City, Akita Prefecture, Japan. We show that negative σ_a is not just a so-called "unphysical quantity" but rather, it can be effective in recovering the underground structure if the data is appropriately processed.

The LIN approximation forms the foundational theory from which LIN-EM instruments are developed. McNeill (1980) gave a detailed account on the assumptions considered at LIN conditions and the derivation of the LIN equations. LIN-EM instruments use measurements of the coupling between two loops, which can be operated in either the VMD or HMD configurations (Fig.1). The *Geonics* instrument measures the quadrature component, and the observed magnetic fields ratio can be converted to apparent conductivity (σ_a) in mS/m (McNeill, 1980).

$$\sigma_a = \frac{4}{\omega \mu_0 s^2} \left(\frac{H_s}{H_p} \right)_Q , \tag{1}$$

where ω is the angular frequency defined as $\omega = 2\pi f$, f is the frequency in Hz, s is the coil separation in metres, and μ_0 is the magnetic permeability of free space, = $4\pi \times 10^{-7}$ Hm^{-1}.

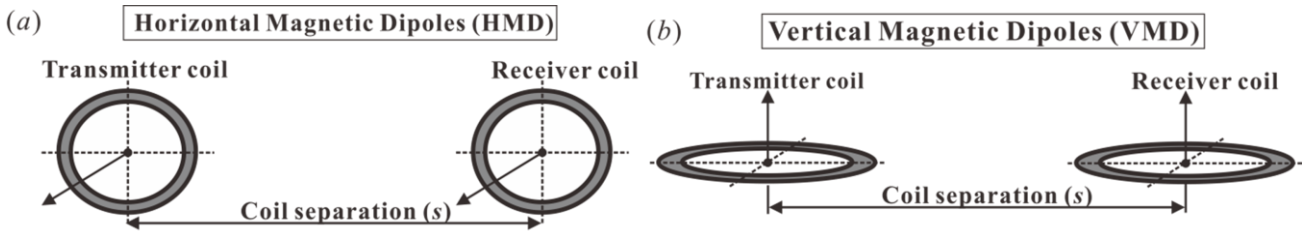

Fig. 1, Illustration of the operation modes of a typical LIN-EM instrument; the coils may be aligned in (*a*) Horizontal Magnetic Dipole (Vertical coplanar), or (*b*) Vertical Magnetic Dipole (Horizontal coplanar) modes as indicated by directional arrows.

THREE DIMENSIONAL WEIGHTING FUNCTION

In this section we present the mathematical formulae that were used in our calculation program. The equations were first derived by Gómez-Treviño (1987) directly from Maxwell's equations at quasi-static conditions. A comprehensive treatment of the 3-D integral equation weighting function has been previously given by Méndez-Delgado et al. (1999), and Pérez-Flores et al. (2001, 2012). The reader is directed to these papers as the derivation and proof of the equations is not in the scope of this paper. The weighting function for the VMD coil configuration is given as

$$W_{Hz}\left(\mathbf{r},\mathbf{r}_1,\mathbf{r}_2\right)=-\frac{16\pi s}{\omega\mu_0 m_z}\left[\mathbf{G}_{Hz}\left(\mathbf{r},\mathbf{r}_2\right)\cdot\mathbf{E}_{Hz}\left(\mathbf{r},\mathbf{r}_1\right)\right], \tag{2}$$

where

$$\mathbf{G}_{Hz}\left(\mathbf{r},\mathbf{r}_2\right)=\frac{1}{4\pi}\left[-\frac{\left(y-y_2\right)}{\left|\mathbf{r}-\mathbf{r}_2\right|^3}\mathbf{i}+\frac{\left(x-x_2\right)}{\left|\mathbf{r}-\mathbf{r}_2\right|^3}\mathbf{j}\right], \tag{3}$$

and

$$\mathbf{E}_{Hz}\left(\mathbf{r},\mathbf{r}_1\right)=-\frac{\omega\mu_0 m_z}{4\pi}\left[-\frac{\left(y-y_1\right)}{\left|\mathbf{r}-\mathbf{r}_1\right|^3}\mathbf{i}+\frac{\left(x-x_1\right)}{\left|\mathbf{r}-\mathbf{r}_1\right|^3}\mathbf{j}\right], \tag{4}$$

and where

$$\left|\mathbf{r}-\mathbf{r}_n\right|=\sqrt{\rho_n^2+\left(z+h\right)^2}, \tag{5}$$

and

$$\rho_n=\sqrt{\left(x-x_n\right)^2+\left(y-y_n\right)^2}\qquad n=1,2\quad , \tag{6}$$

where $\mathbf{r}_1$ is the source location, $\mathbf{r}_2$ is the receiver location, s is the separation distance, h is the height above ground, ω is the angular frequency, μ_0 is the permeability of free space, m_z is the magnetic moment of the dipole source, and unit vectors **i** and **j** are in the x- and y-directions, respectively. $\mathbf{E}_{Hz}(\mathbf{r}, \mathbf{r}_1)$ is the induced electric field within the earth, and $\mathbf{G}_{Hz}(\mathbf{r}, \mathbf{r}_2)$ is the magnetic Green's function of the half-space. The weighting function for the HMD configuration is given by

$$W_{Hy}\left(\mathbf{r},\mathbf{r}_1,\mathbf{r}_2\right)=-\frac{16\pi s}{\omega\mu_0 m_y}\left[\mathbf{G}_{Hy}\left(\mathbf{r},\mathbf{r}_2\right)\cdot\mathbf{E}_{Hy}\left(\mathbf{r},\mathbf{r}_1\right)\right], \tag{7}$$

where

$$\mathbf{G}_{Hy}(\mathbf{r},\mathbf{r}_2)=\frac{1}{4\pi}\left\{\left[\frac{1}{\rho_2^2}-\frac{z+h}{\rho_2^2|\mathbf{r}-\mathbf{r}_2|}-\frac{2(y-y_2)^2}{\rho_2^4}+\frac{2(z+h)(y-y_2)^2}{\rho_2^4|\mathbf{r}-\mathbf{r}_2|}+\frac{(z+h)(y-y_2)^2}{\rho_2^2|\mathbf{r}-\mathbf{r}_2|^3}\right]\mathbf{i}+\left[\frac{(x-x_2)(y-y_2)}{\rho_2^2}\left(\frac{2}{\rho_2^2}-\frac{2(z+h)}{\rho_2^2|\mathbf{r}-\mathbf{r}_2|}-\frac{z+h}{|\mathbf{r}-\mathbf{r}_2|^3}\right)\right]\mathbf{j}\right\}, \tag{8}$$

and

$$\mathbf{E}_{Hy}(\mathbf{r},\mathbf{r}_1)=-\frac{\omega\mu_0 m_y}{4\pi}\left\{\left[\frac{1}{\rho_1^2}-\frac{z+h}{\rho_1^2|\mathbf{r}-\mathbf{r}_1|}-\frac{2(y-y_1)^2}{\rho_1^4}+\frac{2(z+h)(y-y_1)^2}{\rho_1^4|\mathbf{r}-\mathbf{r}_1|}+\frac{(z+h)(y-y_1)^2}{\rho_1^2|\mathbf{r}-\mathbf{r}_1|^3}\right]\mathbf{i}+\left[\frac{(x-x_1)(y-y_1)}{\rho_1^2}\left(\frac{2}{\rho_1^2}-\frac{2(z+h)}{\rho_1^2|\mathbf{r}-\mathbf{r}_1|}-\frac{z+h}{|\mathbf{r}-\mathbf{r}_1|^3}\right)\right]\mathbf{j}\right\}. \tag{9}$$

The integral result of the product of the weighting function, given in equations (2) and (7), with ground conductivity $\sigma(\mathbf{r})$ gives the apparent conductivity as it would be recorded at the surface using a LIN-EM instrument. These are given by equations (10) and (11) for VMD and HMD respectively.

$$\sigma_{a,z}(\mathbf{r}_1,\mathbf{r}_2)=-\frac{16\pi s}{\omega\mu_0 m_z}\int_v\left[\mathbf{G}_{Hz}(\mathbf{r},\mathbf{r}_2)\cdot\mathbf{E}_{Hz}(\mathbf{r},\mathbf{r}_1)\right]\sigma(\mathbf{r})d^3r, \tag{10}$$

$$\sigma_{a,y}(\mathbf{r}_1,\mathbf{r}_2)=-\frac{16\pi s}{\omega\mu_0 m_y}\int_v\left[\mathbf{G}_{Hy}(\mathbf{r},\mathbf{r}_2)\cdot\mathbf{E}_{Hy}(\mathbf{r},\mathbf{r}_1)\right]\sigma(\mathbf{r})d^3r. \tag{11}$$

The resulting images for the 3-D weighting functions for the VMD and HMD configurations are shown in Fig.2. The 3-D weighting functions were calculated assuming the source to be positioned at (-0.5, 0) and the receiver at (0.5, 0). The spatial extents of the calculation were from -1.25 to 1.25 on the *x* and *y* dimensions and 0 to 1 on the *z* dimension.

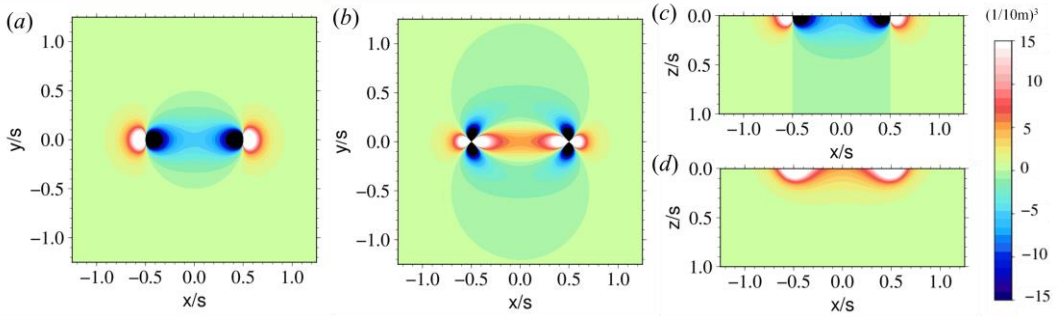

Fig. 2, The 3-D weighting function for the VMD and HMD coil configurations: (*a*) and (*b*) plan view at *z*/*s* = 0, (*c*) and (*d*) cross sectional view at *y*/*s* = 0. The horizontal and vertical scales are normalized by the coil separation *s* and the weighting function by $(1/s)^3$. We calculated for s = 10m therefore the scale of the weighting function is $(1/10\text{m})^3$.

APPLICATION TO FIELD DATA

The study area is an abandoned volcanic tuff quarry in Sugisawa, Daisen City, in the southern part of Akita Prefecture, Japan (Fig.3*a*). Apparent conductivity data shown in Fig.4, were collected by Sasaki (2007) using a *Geonics* EM-34-3 conductivity meter. Negative σ_a anomalies were encountered in VMD

10m and VMD 20m datasets at the south part of the area, anomaly A and the north of the area, anomaly C. The VMD 10m data exhibited a 'horse-shoe' shaped negative σ_a anomaly A. Anomaly C had a similar shape but less defined and lower in magnitude. In the VMD 20m σ_a map, anomaly A had negative σ_a values enclosing two thin regions. Still in the VMD 20m dataset, anomaly B and anomaly C σ_a responses did not reach negative values but rather low σ_a responses.

In order to delineate the subsurface structures responsible for the negative σ_a response, we considered two model case scenarios; 1) a conductor-absent model and 2) a conductor-present model. Different models were calculated and reviewed based on their geophysical and geological merit. The different geoelectrical zones in our trial and error 3-D forward modeling were: the dacite dikes, which were assigned a σ value of 1 mS/m; the high conductivity zones with conductivities from 50-100 mS/m; and the surrounding volcanic tuff bodies were modeled at σ values of 15-35 mS/m. Figure 5(*a*-*c*) is the 3-D models with no conductor, and with conductive bodies set to a 5m and a maximum depth extent of 60 m respectively. From the model response σ_a maps in Fig.6, anomalies A, B and C are visible for both HMD and VMD datasets. To further appreciate the fit of the models we extracted profile B-B' shown in Figs.7, 8 and 9.

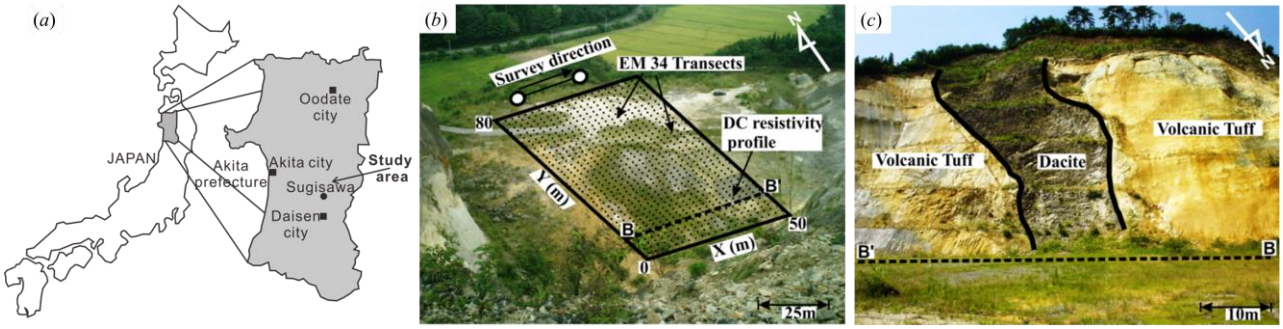

Fig. 3, (*a*) Location of the study area in Sugisawa, Akita Prefecture, Japan, (*b*) Location of the study area showing the survey grid EM-34-3 transects and the DC resistivity profile line, (*c*) the geology of the area and profile B-B' (Photo credit: D. Sasaki).

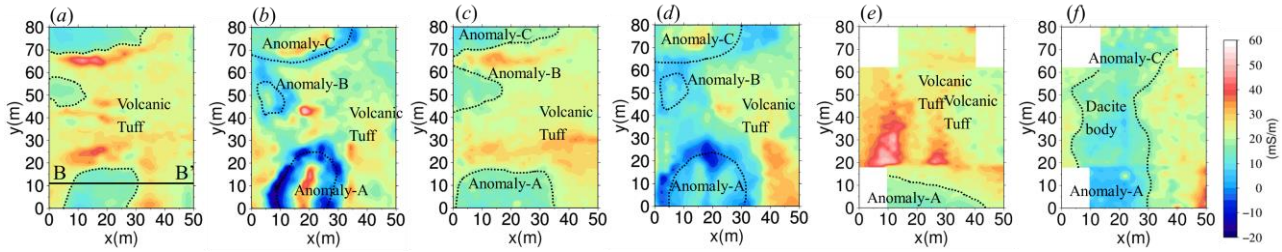

Fig. 4, Spatial distribution of σ_a data collected in the study area (*a*) HMD 10m-obs, (*b*) VMD 10m-obs, (*c*) HMD 20m-obs, (*d*) VMD 20m-obs, (*e*) HMD 40m-obs, (*f*) VMD 40m-obs.

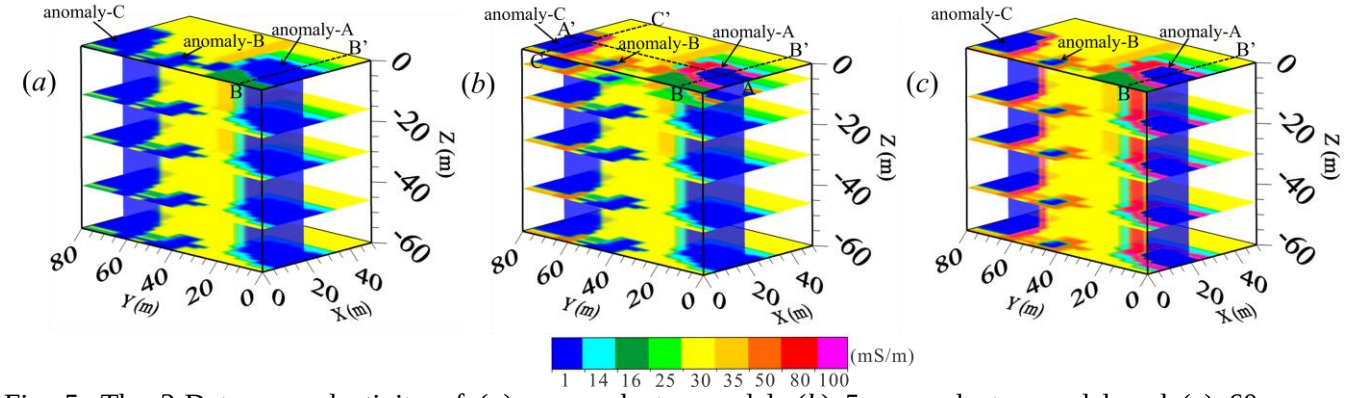

Fig. 5, The 3-D true conductivity of (*a*) no conductor model, (*b*) 5-m conductor model and (*c*) 60-m conductor model.

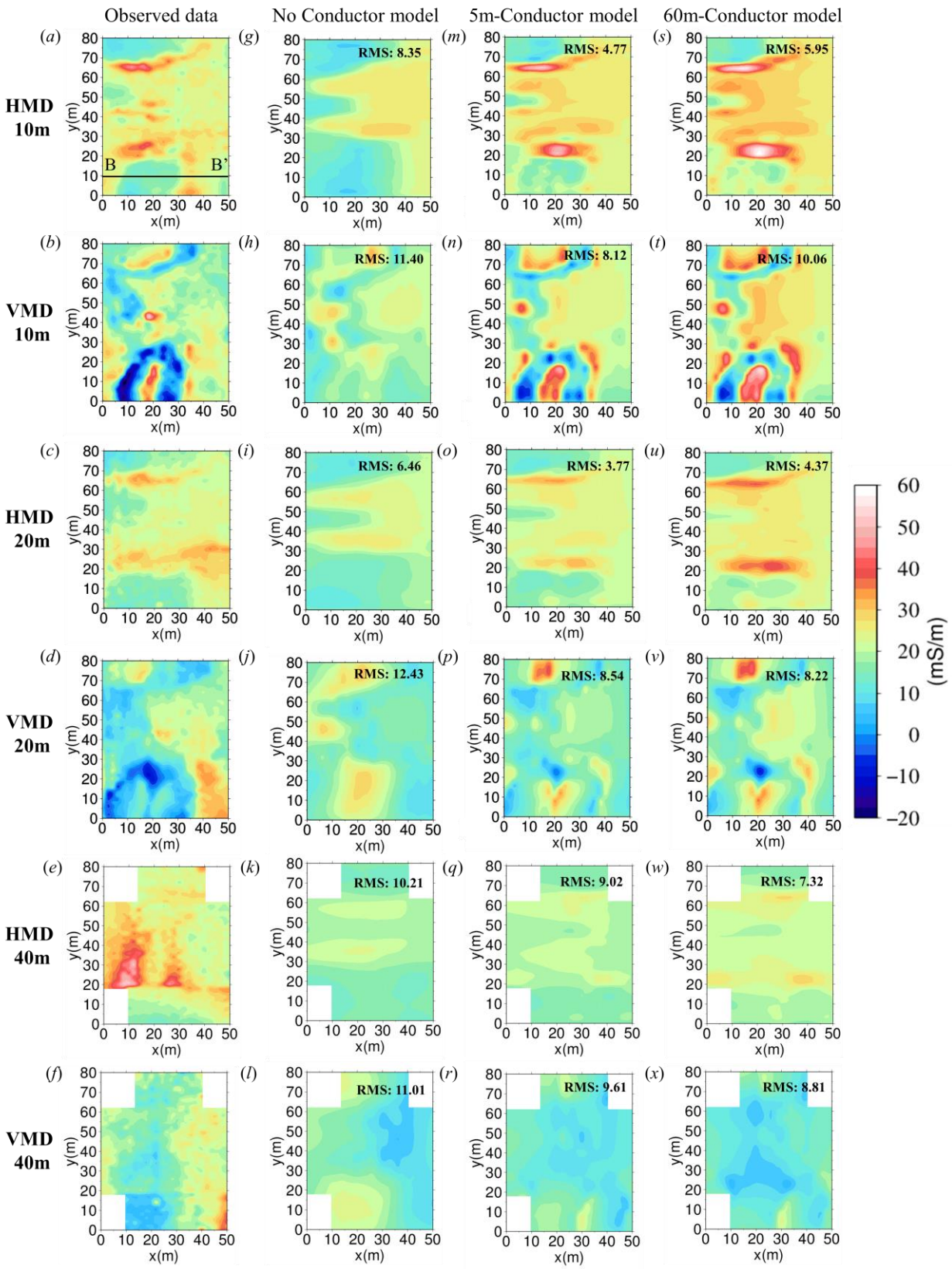

Fig. 6, Spatial distribution of HMD and VMD observed σ_a data (*a-f*), compared with the model responses : (*g-l*) no-conductor model responses, (*m-r*) 5-m-conductor model responses, (*s-x*) 60-m-conductor model responses.

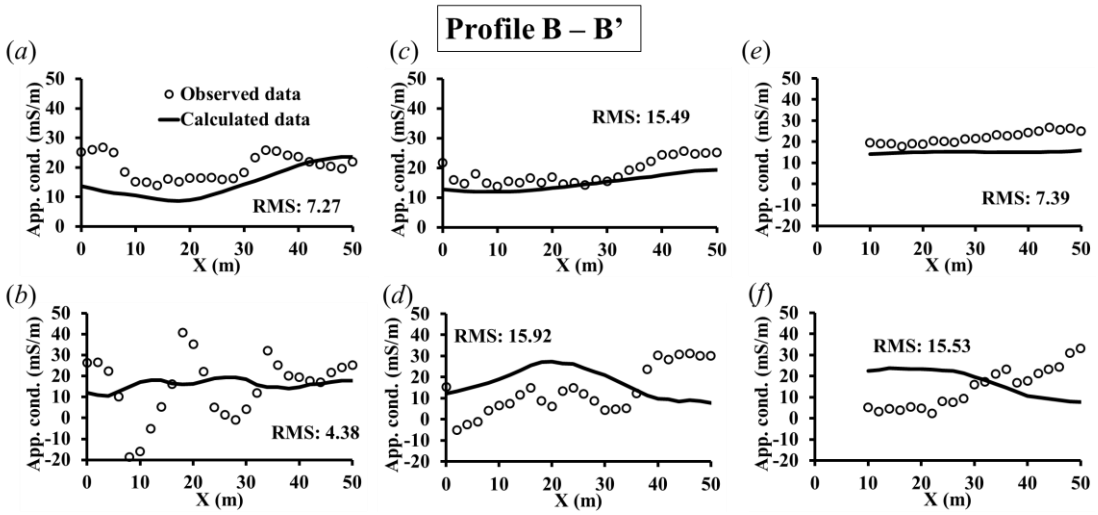

Fig. 7, Observed versus calculated data response curves for the no conductor model across profile B-B' (*a*) HMD 10m, (*b*) VMD 10m, (*c*) HMD 20m, (*d*) VMD 20m, (*e*) HMD 40m, (*f*) VMD 40m.

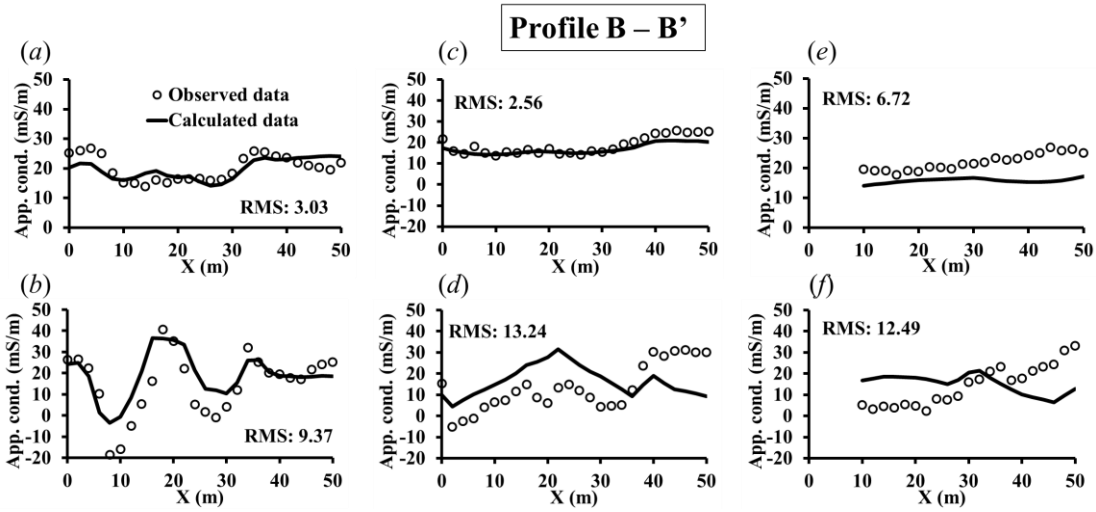

Fig. 8, Observed versus calculated data response curves for the 5m conductor model across profile B-B' (*a*) HMD 10m, (*b*) VMD 10m, (*c*) HMD 20m, (*d*) VMD 20m, (*e*) HMD 40m, (*f*) VMD 40m.

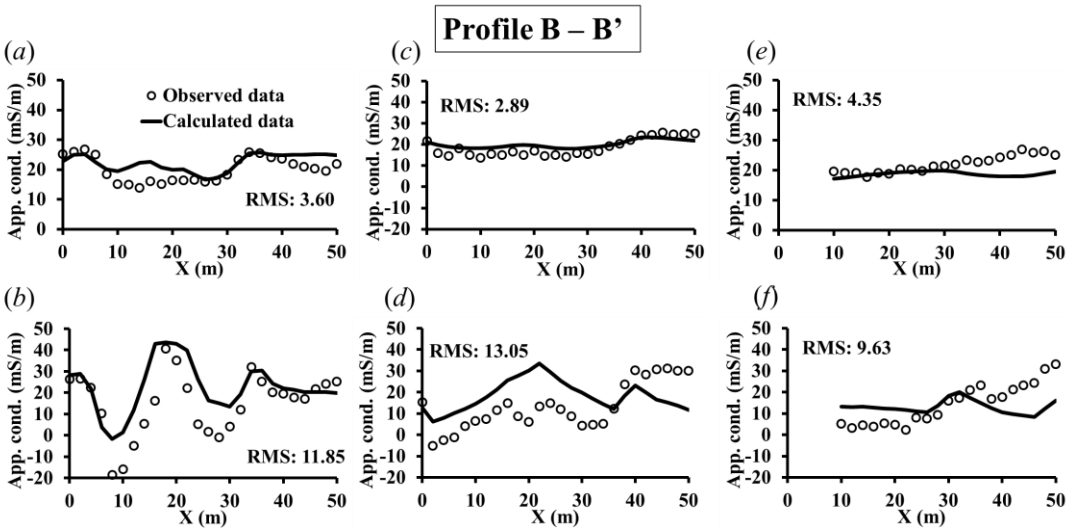

Fig. 9, Observed versus calculated data response curves for the 60m conductor model across profile B-B' (*a*) HMD 10m, (*b*) VMD 10m, (*c*) HMD 20m, (*d*) VMD 20m, (*e*) HMD 40m, (*f*) VMD 40m.

DISCUSSION

The interpretation of the negative σ_a anomalies encountered in the study area was further confirmed by a DC resistivity survey. Profile B-B' in Fig.10 shows the 2-D inversion section of the resistivity data. The low conductivity zone from 14-28 m is interpreted to represent the dacite dike. The moderately conductive zones occur to the left and far right of the section are thought to represent the surrounding volcanic tuff. The highly conductive zones occur between 8-14 m and 28-39 m on both sides of the low conductivity dike. Our model also includes these highly conductive zones (50-100 mS/m) that correspond to the negative σ_a anomalies encountered in the area. It can be observed that the DC resistivity survey conductivity model values for these three zones fall within the range estimated by our 3-D forward model.

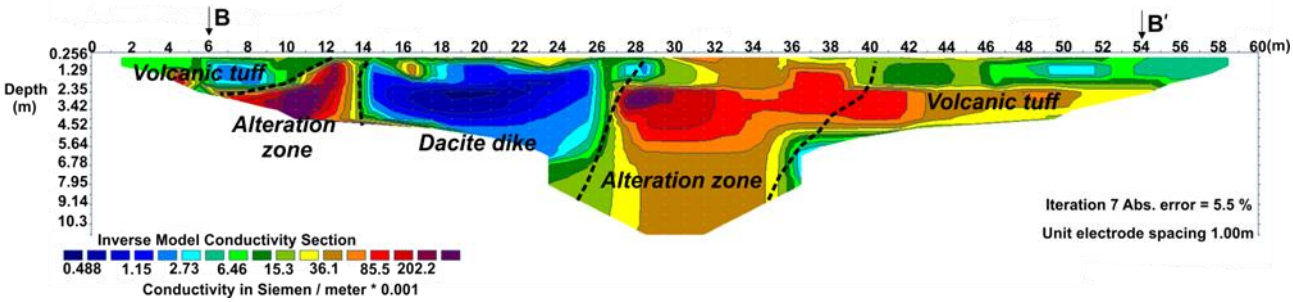

Fig. 10, Inverse model of DC resistivity data along profile line B-B'.

CONCLUSION

We extended the findings by Pérez-Flores et al. (2012) by using the 3-D weighting function, based on the LIN approximation, to model real field data exhibiting negative σ_a anomalies. We performed 3-D forward modeling on the data and successfully calculated negative σ_a responses. We have shown that negative σ_a, widely regarded as an unphysical quantity, can be an effective observation in recovering the subsurface structure.

ACKNOWLEDGEMENTS

Parts of this paper has been submitted for publication in *Exploration Geophysics* and have been presented at *the 130th, 131st and 132nd SEGJ Conferences.* Our calculation programs were coded using *Microsoft Visual Studio C# 2012 Express Edition*.

REFERENCES

Gómez-Treviño, E., 1987, Nonlinear integral equations for electromagnetic inverse problems: *Geophysics*, **52**, 1297-1302. doi:10.1190/1.1442390.

Méndez-Delgado, S., Gómez-Treviño, E., and Pérez-Flores, M. A., 1999, Forward modeling of direct current and low frequency electromagnetic fields using integral equations: *Geophysical Journal International*, **137**, 336-352. doi:10.1046/j.1365-246X.1999.00826.x.

McNeill, J. D., 1980, *Electromagnetic terrain conductivity measurement at low induction numbers*: Technical note TN-6 (unpublished), Geonics Limited, Canada.

McNeill, J. D., 1983, *EM 34-3 Survey Interpretation Techniques*: Technical note TN-8 (unpublished), Geonics Limited, Canada.

Pérez-Flores, M. A., Méndez-Delgado, S., and Gómez-Treviño, E., 2001, Imaging of low-frequency and DC electromagnetic fields using a simple linear approximation: *Geophysics*, **66**, 1067-1081. doi:10.1190/1.1487054.

Pérez-Flores, M. A., Antonio-Carpo, R. G., Gómez-Treviño, E., Ferguson, I., and Méndez-Delgado, S., 2012, Imaging of 3-D electromagnetic data at low-induction numbers: *Geophysics*, **77**, no. 4, WB47-WB57. doi:10.1190/geo2011-0368.1.

Sasaki, D., 2007, *Electrical conductivity structure analysis by electromagnetic survey*: M.Sc. thesis (unpublished), Akita University (in Japanese with English abstract).